Integrated Ferroelectrics
An International Journal

ISSN: 1058-4587 (Print) 1607-8489 (Online) Journal homepage: http://www.tandfonline.com/loi/ginf20

Increasing the fill factor of inverted polymer bulk heterojunction solar cells by doping PVP modified $NaYF_4$ nanoparticles

Xiande Wang, Ya'nan Zou, Yupeng Xie, Changhao Wang, Fanxu Meng, Liang Sun, Chuan Chen & Shengping Ruan

To cite this article: Xiande Wang, Ya'nan Zou, Yupeng Xie, Changhao Wang, Fanxu Meng, Liang Sun, Chuan Chen & Shengping Ruan (2017) Increasing the fill factor of inverted polymer bulk heterojunction solar cells by doping PVP modified $NaYF_4$ nanoparticles, Integrated Ferroelectrics, 180:1, 168-174, DOI: 10.1080/10584587.2017.1340710

To link to this article: https://doi.org/10.1080/10584587.2017.1340710

Published online: 29 Sep 2017.

INTEGRATED FERROELECTRICS
2017, VOL. 180, 168–174
https://doi.org/10.1080/10584587.2017.1340710

Taylor & Francis
Taylor & Francis Group

Increasing the fill factor of inverted polymer bulk heterojunction solar cells by doping PVP modified $NaYF_4$ nanoparticles

Xiande Wang[a], Ya'nan Zou[a], Yupeng Xie[a], Changhao Wang[a], Fanxu Meng[a], Liang Sun[b], Chuan Chen[b], and Shengping Ruan[b]

[a]Jilin Institute of Chemical Technology, People's Republic of China; [b]State Key Laboratory on Applied Optics and Global Energy Interconnection Research Institute, People's Republic of China

ABSTRACT

$NaYF_4$ nanoparticles (NPs), synthesized by a facile solvothermal approach using polyvinylpyrrolidone (PVP) as a surfactant, were doped into P3HT:PCBM blend to fabricate inverted polymer bulk heterojunction solar cells. The results showed that the fill factor (FF) of the device was greatly enhanced by doping $NaYF_4$ NPs/PVP composites into the active layer. There were evidences that PVP can form charge transfer (CT) complexes with PCBM. And the CT complexes, formed by PCBM and PVP carried by $NaYF_4$ NPs, might make contributions to the phase separation of the active layer (P3HT:PCBM blend), which is vital to the *FF* of the devices.

ARTICLE HISTORY
Received 13 September 2016
Accepted 7 March 2017

KEYWORDS
Fill factor; charge transfer; polymer solar cells

1. Introduction

Solution-processed bulk heterojunction (BHJ) polymer solar cells (PSCs) are considered to be an exciting class of next-generation photovoltaics, due to their great probability of the realization of low cost, mechanically flexible, light weight, large-area devices that can be fabricated by room-temperature solution processing [1, 2]. Recently, efficiencies of ~9–10% have been reported with low band gap polymers as electron donors [1, 3–4]. In spite of this the power conversion efficiency (PCE) of PSCs is still not high enough for commercial use. The morphology of the active layer plays an important role on the performance of PSCs, especially on the fill factor (*FF*) of the devices. Much efforts, such as thermal annealing [5], solvent drying [6], or addition of chemical additives [7], have been engaged in improving the phase separation of the active layer. It is noteworthy that the phase separation of the active layer can also be tuned through the incorporation of inorganic nanoparticles (INPs) into the blend films, and this could apparently improve the performance of PSCs as

CONTACT Fanxu Meng fxmengjlu@gmail.com Jilin Institute of Chemical Technology, People's Republic of China; Shengping Ruan Ruansp@jlu.edu.cn State Key Laboratory on Applied Optics and Global Energy Interconnection Research Institute, People's Republic of China.
Color versions of one or more of the figures in the article can be found online at www.tandfonline.com/ginf.

a result [8, 9]. However, the mechanism behind this would change with the various properties of different INPs.

In this paper, we provide a new approach to enhance the *FF* of inverted P3HT:PCBM PSCs. Cubic phase $NaYF_4$ nanoparticles (NPs) was prepared by a facile solvothermal method using polyvinylpyrrolidone (PVP) as a surfactant. Then the NPs were doped into the P3HT:PCBM blend film. The NPs have an average size of ~40 nm and can be well dispersed in the BHJ solution. The device performances with and without NPs were both investigated and compared. The *FF* of inverted PSCs can be enhanced by incorporating PVP modified $NaYF_4$ NPs into P3HT:PCBM blend film while improving the short-circuit current density (J_{sc}) and open-circuit voltage (V_{oc}).

2. Experimental details

For the synthesis of $NaYF_4$ NPs, 0.5 g PVP K-30 (58,000 g mol^{-1}) was dissolved in 8 mL ethylene glycol (EG, AR) under stirring. As followed, 0.24 g $YCl_3 \cdot xH_2O$ (99.99%, Alfa Aesar) was added and dispersed still under stirring. This solution was labeled as solution I. 0.23 g sodium fluoride (NaF, AR) was dissolved in 10 mL EG and added dropwise to solution I. Then the solution was kept stirring for at least 30 min and subsequently transferred into a polytetrafluoroethylene autoclave, followed by being heated at 150°C for 24 h. After cooling down to room temperature, the as-product was obtained by centrifugation and washed with deionized (DI) water and ethanol. Finally, the precipitation was dried at 60°C.

It has been reported that the inverted PSCs exhibit the advantages of utilizing the spontaneous vertical phase separation of the active layer, i.e. spontaneous vertical stratification upon spin-coating the polymer films, as well as the enrichment of the donor and acceptor components at the top and bottom surfaces, respectively [10,11]. Hence the devices were fabricated with the inverted structure of indium tin oxide (ITO)/nano-crystal titanium dioxide (nc-TiO_2)/P3HT:PCBM:$NaYF_4$ NPs/sliver (Ag). The nc-TiO_2 film on the cathode ITO side is an electron-selective layer, and Ag works as the anode to collect the holes. Therefore the device works inverted. Patterned ITO-coated glass substrates were sonicated consecutively with acetone, isopropyl alcohol, and DI water for 10 min, respectively. TiO_2 thin films were subsequently prepared as described in our previous papers [12]. For the active layer, the 1,2-dichlorobenzene (DCB) solution composed of P3HT (15 mg mL^{-1}), PCBM (15 mg mL^{-1}), and $NaYF_4$ NPs (x mg mL^{-1}, x = 0, 6) was spin-cast at 700 rpm on top of the nc-TiO_2 layer in air. P3HT and PCBM were purchased from Lumtec Corp. and used without further purification. Then the samples were baked in low vacuum (vacuum oven) at 150°C for 10 min. Finally, the devices were completed with thermal evaporation of Ag electrode. The active area of the device was about 0.064 cm^2.

X-ray diffraction (XRD) analysis of $NaYF_4$ NPs powder was carried out with a powder diffractometer (Model Rigaku RU-200b), using Ni-filtered Cu Kα radiation ($\lambda = 1.5406$ Å) with 200 mA current and 50 kV voltage across the tube to generate powerful X-ray. The XRD measurement was performed at a scan rate of

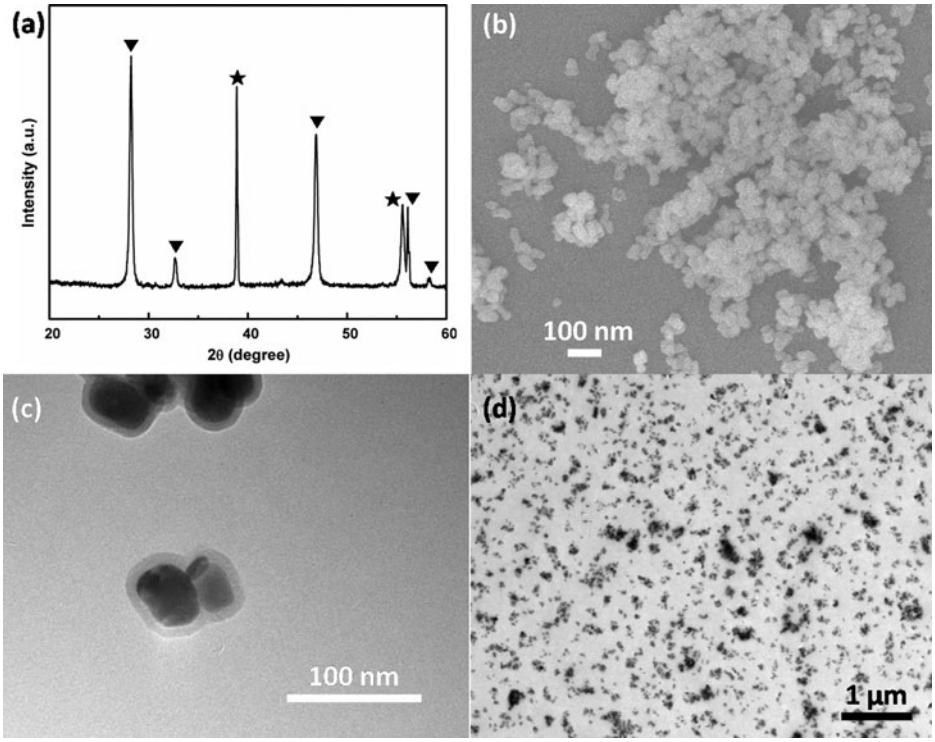

Figure 1. (a) XRD pattern of the as-prepared $NaYF_4$ NPs. (b) SEM and (c) TEM images of the $NaYF_4$ NPs. (d) TEM image of P3HT: PCBM blend film doped with $NaYF_4$ NPs annealed at 150°C for 10 min.

18° min^{-1} and step size of 0.02°. The morphology of $NaYF_4$ nano-crystals and the blend film with $NaYF_4$ NPs was investigated by TEM (Hitachi, H-600 100KV) and FE-SEM (JEOL, JSM-7500F). A 100 W xenon lamp equipped in the Hitachi F-4500 fluorescence spectrophotometer was used as the PL pump source. The PL spectra of the BHJ films were recorded in the same condition with a Hitachi F-4500 fluorescence spectrophotometer [450 nm for excitation wavelength, 5.0 nm for spectral resolution (FWHM) of the spectrophotometer and 400 V for PMT voltage] at room temperature. Current density–voltage (*J*–*V*) characteristics of PSCs were measured with a computer-programmed Keithley 2400 source/meter under AM 1.5 G solar illuminations with an Oriel 300 W solar simulator intensity of ~100 mW cm^{-2} in air without encapsulation. The light intensity was measured with a photometer (International light, IL1400) corrected by a standard silicon solar cell. The absorption spectra were measured by means of ultraviolet/visible spectrometer (UV 1700, Shimadzu).

3. Results and discussion

The XRD pattern of $NaYF_4$ sample is shown in Fig. 1(a), where the diffraction peaks labeled by (▼) are in good agreement with the data of cubic-phase $NaYF_4$ nanocrystals (JCPDS No. 06–0342, $\alpha = 5.448$ Å), indicating the pure cubic $NaYF_4$ crystals and highly crystalline nature of $NaYF_4$. However, the diffraction peaks labeled by (⋆) are in accordance with the data of NaF (JCPDS No. 01–1184), and this indicates

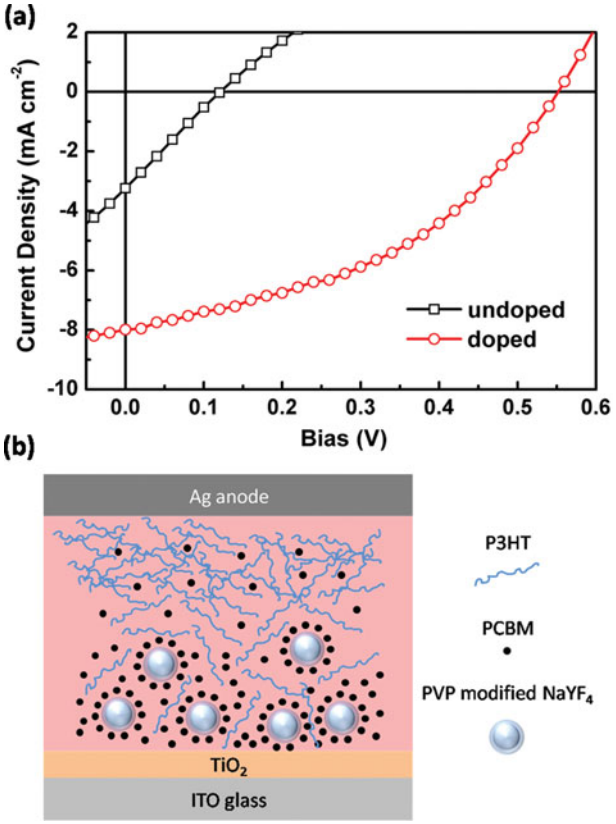

Figure 2. (a) The *J-V* characteristics of the doped and undoped devices under AM1.5 G illumination with the intensity of 100 mW cm^{-2} in ambient air. (b) The device structure of the inverted polymer solar cells.

the existing of some unreacted NaF. Figures 1(b) and (c) show the SEM and TEM images of the cubic phase $NaYF_4$ crystals. It can be estimated that the as-prepared $NaYF_4$ NPs have an average size of ~40 nm. Since both the nitrogen and oxygen atoms of PVP have lone pair electrons which can combine with the empty orbital of metal ions, it has been reported that PVP can act as a chelating agent and coordinate with Y^{3+} in the reaction process [13]. As a result, the NPs are capped by PVP [Fig. 1(c)]. After the formation of NPs, PVP serves as a surfactant and drives the NPs to be dispersed in DCB solution. The TEM image [Fig. 1(d)] of P3HT: PCBM: $NaYF_4$ NPs blend film reveals that some NPs aggregate into small clusters and most of NPs are uniformly dispersed in the BHJ film after being annealed at 150°C for 10 min.

Figure 2(a) shows *J-V* characteristics of the devices with and without $NaYF_4$ NPs under AM 1.5G illumination with the intensity of 100 mW cm^{-2} in ambient air. The control device without NPs exhibits a J_{sc} of 3.24 mA cm^{-2}, V_{oc} of 0.12 V, *FF* of 25.7%, leading to a PCE of 0.10%. However, the device doped with NPs exhibits a better PCE of 1.84% with J_{sc} of 7.99 mA cm^{-2}, V_{oc} of 0.55 V, and a much higher *FF* of 41.8%. The detailed results are summarized in Table 1. By the introduction of $NaYF_4$ NPs, the series resistance of the device, which is defined by the slope of the

Table 1. Device performance, including short-circuit current density (J_{sc}), open-circuit voltage (V_{oc}), fill factor (*FF*), and power conversion efficiency (PCE), dependent on the introduction of $NaYF_4$ NPs.

Device	J_{sc} (mA/cm^2)	V_{oc} (V)	*FF* (%)	PCE(%)
Undoped	3.24	0.12	25.7	0.10
Doped	7.99	0.55	41.8	1.84

J-V curve at $J = 0$ mA/cm^2 under illumination, falls to ~23.27 Ω·cm^{-2} compared with ~40.91 Ω·cm^{-2} of the device without NPs. And it contributes partly to the increase in *FF*. However, the shunt resistant of the device with NPs, which is defined by the slope of the *J-V* curve at $V = 0$ V under illumination, increases to ~282.33 Ω·cm^{-2} compared with ~38.43 Ω·cm^{-2} of the device without NPs. The elevated shunt resistance also makes contribution to the improvement in *FF*.

Considering the devices without an electron-selective layer, both P3HT and PCBM are in direct contact with Ag. It is possible for PCBM to transfer electrons to the Ag electrode resulting in the strong recombination of carriers, thereby compromising the *FF* and efficiency of device [12]. Nevertheless, PVP has been demonstrated to form charge transfer (CT) complexes with C_{60} due to the CT interaction of PVP functional groups with the C_{60} surface [14–16]. As a derivative of C_{60}, PCBM can be reasonably considered to form the CT complexes with PVP on the surface of $NaYF_4$ NPs. Therefore, as shown in Fig. 2(b), the enrichment of PCBM at the bottom surface will be enhanced by the bonding of CT state between PCBM and PVP, which occurs with the uniformly dispersing and precipitating of NPs in the active layer during the thermal annealing. Moreover, the formation of isolated islands of PCBM clusters could be reduced, and the effective contact area of PVP/PCBM and P3HT/PCBM would increase. As a result, for the device doped with NPs, the recombination of carriers can be effectively weakened at Ag anode side, leading to an improvement of *FF*. In addition, J_{sc} and V_{oc} of the device with NPs can be also improved due to the strengthened transformation and accumulation of carriers towards the corresponding electrode. Figure 3 shows the dark *J-V* curves of inverted

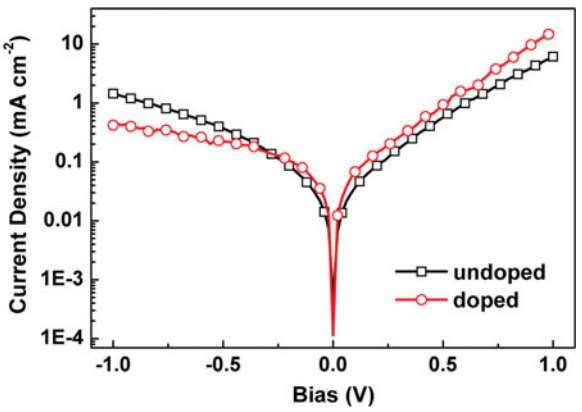

Figure 3. The *J-V* characteristics of the doped and undoped devices in dark.

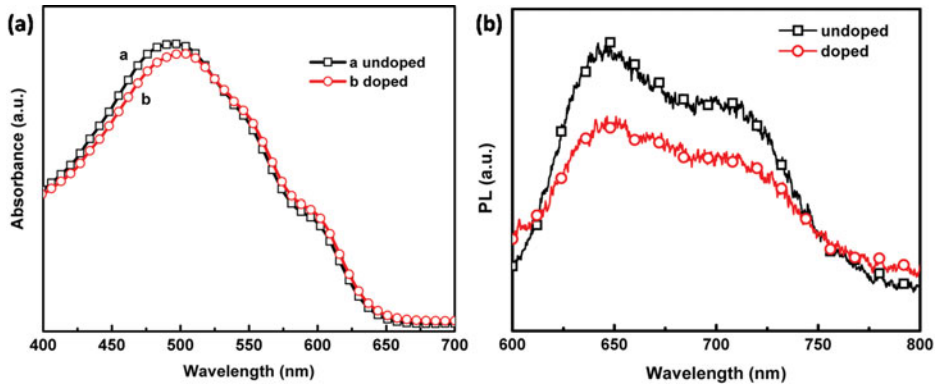

Figure 4. (a) The absorption spectra of the doped and undoped active layers. (b) PL spectra of the doped and undoped BHJ films annealed at 150°C for 10 min.

PSCs with and without NPs. The device with NPs exhibits a higher current rectification ratio of 38.72 at ±1 V compared to 4.25 for the device without NPs. It means that the device with NPs exhibits a better rectifying performance than that of the device without NPs. This significantly evidences that the *FF* can be enhanced by doping PVP modified $NaYF_4$ NPs.

The photoluminescence (PL) is measured to further examine the exciton dissociation in the BHJ films. Figure 4(b) shows the PL spectra of the BHJ films with and without NPs annealed at 150°C for 10 min. The PL signals are corrected with the absorption spectra of the BHJ films at wavelength of 450 nm [Fig. 4(a)]. PL quenching is observed for the BHJ film with NPs comparing to that without NPs. This provides direct evidence for enhanced exciton dissociation and reduced electron/hole recombination by incorporating the NPs, resulting in the improvement in the performance of PSCs.

4. Conclusion

In conclusion, PVP modified cubic-phase $NaYF_4$ nanoparticles with an average size of ~40 nm are synthesized by a facile solvothermal approach. The PSCs exhibit an overall PCE of 1.84% by incorporating $NaYF_4$ NPs into the P3HT:PCBM blend films. The introduction of PVP carried by $NaYF_4$ NPs enhances *FF* from 25.7% to 41.8% via the formation of CT complexes with PCBM, and thus makes contributions to vertical phase separation of the active layer. Simultaneously, the insertion of NPs improves both J_{sc} and V_{oc}, leading to the overall efficiency improvement.

Acknowledgements

This work was supported by the National Natural Science Foundation of China (Grant Nos. 11574110, 11447194), Project of Statistic Analysis of Gas Sensitive Materials, Opened Fund of the State Key Laboratory on Applied Optics, and Scientific Research Fund of Jilin Provincial Education Department (2015437).

References

1. Z. He, B. Xiao, F. Liu, H. Wu, Y. Yang, S. Xiao, C. Wang, T. P. Russell, and Y. Cao, Single-junction polymer solar cells with high efficiency and photovoltage. *Nature Photon.* **9**, 174–179 (2015).
2. J. Wang, Y. Wang, D. He, H. Wu, H. Wang, P. Zhou, and M. Fu, Influence of polymer/fullerene-graphene structure on organic polymer solar devices. *Integrated Ferroelectrics* **137**, 1–9 (2012).
3. Z. He, C. Zhong, S. Su, M. Xu, H. Wu, and Y. Cao, Enhanced power-conversion efficiency in polymer solar cells using an inverted device structure. *Nature Photon.* **6**, 591–595 (2012).
4. S. H. Liao, H. J. Jhuo, Y. S. Cheng, and S. A. Chen, Fullerene derivative-doped zinc oxide nanofilm as the cathode of inverted polymer solar cells with low-bandgap polymer (PTB7-Th) for high performance. *Adv. Mater.* **25**, 4766–4771 (2013).
5. T. Erb, U. Zhokhavets, G. Gobsch, S. Raleva, B. Stühn, P. Schilinsky, C. Waldauf, and C. J. Brabec, Correlation between structural and optical properties of composite polymer/fullerene films for organic solar cells. *Adv. Func. Mater.* **15**, 1193–1196 (2005).
6. G. Li, V. Shrotriya, J. Huang, Y. Yao, T. Moriarty, K. Emery, and Y. Yang, High-efficiency solution processable polymer photovoltaic cells by self-organization of polymer blends. *Nat. Mater.* **4**, 864–868 (2005).
7. J. Peet, C. Soci, R. C. Coffin, T. Q. Nguyen, A. Mihailovsky, D. Moses, and G. C. Bazan, Method for increasing the photoconductive response in conjugated polymer/fullerene composites. *Appl. Phys. Lett.* **89**, 252105–252105–3 (2006).
8. C. W. Lin, D. Y. Wang, Y. T. Wang, C. C. Chen, Y. J. Yang, and Y. F. Chen, Increased photocurrent in bulk-heterojunction solar cells mediated by FeS_2 nanocrystals. *Sol. Energy Mater. Sol. Cells* **95**, 1107–1110 (2011).
9. H. C. Liao, C. S. Tsao, T. H. Lin, M. H. Jao, C. M. Chuang, S. Y. Chang, Y. C. Huang, Y. T. Shao, C. Y. Chen, C. J. Su, U. S. Jeng, Y. F. Chen, and W. F. Su, Nanoparticle-tuned self-organization of a bulk heterojunction hybrid solar cell with enhanced performance. *ACS Nano* **6**, 1657–1666 (2012).
10. Z. Xu, L. M. Chen, G. Yang, C. H. Huang, J. Hou, Y. Wu, G. Li, C. S. Hsu, and Y. Yang, Vertical phase separation in poly(3-hexylthiophene):fullerene derivative blends and its advantage for inverted structure solar cells. *Adv. Funct. Mater.* **19**, 1227–1234 (2009).
11. L. M. Chen, Z. Hong, G. Li, and Y. Yang, Recent progress in polymer solar cells: manipulation of polymer:fullerene morphology and the formation of efficient inverted polymer solar cells. *Adv. Mater.* **21**, 1434–1449 (2009).
12. C. Tao, S. Ruan, X. Zhang, G. Xie, L. Shen, X. Kong, W. Dong, C. Liu, and W. Chen, Performance improvement of inverted polymer solar cells with different top electrodes by introducing a MoO_3 buffer layer. *Appl. Phys. Lett.* **93**, 193307–193307-3 (2008).
13. H. Chen, X. Zhai, D. Li, L. Wang, D. Zhao, and W. Qin, Water-soluble Yb^{3+}, Tm^{3+} codoped $NaYF_4$ nanoparticles: synthesis, characteristics and bioimaging. *Alloys Compd.* **511**, 70–73 (2012).
14. C. Ungurenasu, and A. Airinei, Highly stable C_{60}/poly(vinylpyrrolidone) charge-Transfer complexes afford new predictions for biological applications of underivatized fullerenes. *J. Med. Chem.* **43**, 3186–3188 (2000).
15. E. Tarabukina, Z. Zoolshoev, E. Melenevskaya, and T. Budtova, Delivery of fullerene-containing complexes via microgel swelling and shear-induced release. *Int. J. Pharm.* **384**, 9–14 (2010).
16. M. Behera, and S. Ram, Solubilization and stabilization of fullerene C_{60} in presence of poly(vinyl pyrrolidone) molecules in water. *J. Incl. Phenom. Macrocycl. Chem.* **72**, 233–239 (2012).